Automated counting of mammalian cell colonies

**Paul R Barber, Borivoj Vojnovic, Jane Kelly, Catherine R Mayes,
Peter Boulton, Michael Woodcock and Michael C Joiner**

Gray Laboratory Cancer Research Trust, PO Box 100, Mount Vernon Hospital, Northwood,
Middlesex HA6 2JR, UK

E-mail: barber@graylab.ac.uk

Abstract
Investigating the effect of low-dose radiation exposure on cells using assays
of colony-forming ability requires large cell samples to maintain statistical
accuracy. Manually counting the resulting colonies is a laborious task in
which consistent objectivity is hard to achieve. This is true especially with
some mammalian cell lines which form poorly defined or 'fuzzy' colonies,
typified by glioma or fibroblast cell lines. A computer-vision-based automated
colony counter is presented in this paper. It utilizes novel imaging and image-
processing methods involving a modified form of the Hough transform. The
automated counter is able to identify less-discrete cell colonies typical of
these cell lines. The results of automated colony counting are compared with
those from four manual (human) colony counts for the cell lines HT29, A172,
U118 and IN1265. The results from the automated counts fall well within the
distribution of the manual counts for all four cell lines with respect to surviving
fraction (SF) versus dose curves, SF values at 2 Gy (SF_2) and total area under
the SF curve (Dbar). From the variation in the counts, it is shown that the
automated counts are generally more consistent than the manual counts.

1. Introduction

Specialized clonogenic assays have made it possible to examine the response of mammalian
cellular systems to radiation with sufficient accuracy to resolve changes in radiosensitivity at
doses much less than 1 Gy where cell survival approaches 100%. These accurate colony-
forming assays rely on determining precisely the number of cells that are 'at risk' either
by the use of a fluorescence-activated cell sorter (FACS) to *plate* an exact number of cells
(Wouters and Skarsgard 1994, Short and Joiner 1998, Short *et al* 1999a, b) or microscopic
scanning to identify an exact number of cells *after* plating (Marples and Joiner 1993, Spadinger
and Palcic 1993). However, manual counting of the cell colonies from either type of assay
remains tedious, time-consuming and resource-intensive, considering that high cell numbers
are required to achieve acceptable statistical accuracy. In addition to this, manual counting can
be subjective and it has been observed that results can differ between counting personnel (see
for example Lumley *et al* (1997)). The development of a reliable automated colony counter

would reduce the time and resources required to perform such clonogenic assays. Furthermore, automatic methods offer objectivity together with possibilities for greater throughput over extended periods. Combined, these factors allow greater statistical accuracy and minimize the error between comparable experiments.

The concept of computer-aided colony counting is not new and has been implemented by other groups (Thielmann and Hagedorn 1985, Parry *et al* 1991, Wilson 1995, Mukherjee *et al* 1995, Hoekstra *et al* 1998, Dobson *et al* 1999). Several authors have noted the problems associated with detecting colonies around the periphery of a culture flask and several have resorted to masking this area to exclude it from processing. Counting colonies that merge into one another has also proved to be problematic, and statistical corrections have been employed to reduce systematic errors (Thielmann and Hagedorn 1985). Approaches to overcome the problems of merging and less-discrete or fuzzy colonies giving multiple counts have resulted in total-colony-area based statistical counts (Mukherjee *et al* 1995). Image-processing algorithms based on grey-level thresholding have been previously applied to the colony counting problem. This technique alone is not able to disregard the flask edge nor is it suitable for less-discrete colonies. More sophisticated algorithms based on grey-level watersheds have also been tried but these tend to be computationally intensive, and give rise to multiple counts when presented with fuzzy colonies.

Since cell colonies tend to have some affinity for areas around the flask edge it seems unreasonable to exclude these areas, as a reduction in statistical accuracy will result. Merged and fuzzy colonies should also be treated correctly, without the need for statistical correction or estimation. This paper describes an automated colony counter that uses algorithms robust to the problems described above. Also presented is the evaluation of the automatic colony counter against four manual counts from skilled personnel.

2. Materials and methods

The automated colony counter was tested with four cell types, HT29, A172, U118 and IN1265, and the automated results were compared with those of manual counts from four experienced staff at the Gray Laboratory.

2.1. Flask preparation

2.1.1. Cell culture. Cell lines HT29, A172 and U118 were obtained from the European Collection of Animal Cell Cultures (ECACC) and were derived originally from a grade I primary human colon adenocarcinoma, human glioblastoma and grade III astrocytoma–glioblastoma respectively. The IN1265 was supplied by Dr J Darling, Institute of Neurology, London, UK and was derived originally from a primary human glioma. All cells were maintained in monolayer culture *in vitro* in Eagle's minimum essential medium with Earles salts (Sigma-Aldrich Co. Ltd, UK) supplemented with 10% foetal calf serum, 2 mM L-Glutamine, sodium bicarbonate, 1 mM sodium pyruvate, 50 IU ml^{-1} penicillin and 50 μg ml^{-1} streptomycin. All cells were grown in an atmosphere of 90% N_2, 5% CO_2, 5% O_2 and passaged routinely once a week using a calcium-free salt solution containing 0.05% trypsin and 0.02% EDTA.

2.1.2. Cell sorting. Cells were sorted using a FACSVantage cell sorter in conjunction with CellQuest software (Becton-Dickinson, San Jose, CA). Cells were characterized based on their forward-scatter fluorescence (cell 'size') and side-scatter fluorescence (cell 'granularity') and the desired population gated and sorted into T25 tissue-culture flasks (Greiner

Labortechnik, UK) each containing 5 ml of pre-warmed, pre-gassed culture medium. The number of cells actually deflected (sorted) was recorded flask by flask and used to calculate subsequent surviving fractions. Following cell sorting, flasks were returned to the incubator for at least 1 h to allow cells to attach to the growth surface.

2.1.3. Irradiation. Once attached, the cells were irradiated with x-rays generated by a Pantak unit operating at 240 kVp. Filtration of 0.25 mm Cu + 1 mm Al gave an HVL of 1.3 mm Cu at a dose rate of 0.2–0.4 Gy min^{-1}. This was chosen to ensure exposure times of at least 15 s and hence accurate dosimetry in the low-dose range. Cell survival was determined after single doses of up to 5 Gy but focusing on survival at doses less than 1 Gy. Following irradiation, flasks were returned to the incubator and left for 14 days to allow colony formation.

2.1.4. Staining of colonies. The colonies formed were stained using crystal violet (Sigma-Aldrich Co. Ltd, UK) at 20 mg ml^{-1} in 95% ethanol (Hayman, Essex, UK). The growth medium was first decanted and replaced with sufficient stain to overlay the bottom of the flask. After approximately 20–30 min, the stain was removed by immersing the flasks three times under running cold water and the flasks were left to dry in air before colony counting proceeded.

2.1.5. Measurement of cell survival. Cell survival was measured according to the usual criterion of 50 cells or more per colony (Puck and Marcus 1956) with either the automated colony counter or manually by the four observers using a Stuart Scientific colony counter. For these experiments the adherence of the automated counter to the 50 cell criterion was determined by the user by appropriate parameter selection. Surviving fraction (SF) was calculated by dividing the plating efficiency (PE) of irradiated cells by the PE of the cell population of sham-irradiated cells.

2.2. Hardware

The hardware that we have developed incorporates a number of novel features which allow us to obtain high-quality images of the whole flask, including the flask corners. The system consisted of a monochrome camera with 1/3" format CCD with a wide-angle lens of 2.8 mm focal length, which produced a field of view of 75 by 56 mm in the plane of the bottom of the culture flask. The bottom of the flask was at a distance of 62 mm from the lens flange (C-mount). We operated with the lens aperture fully opened ($f/1.6$) such that the depth of focus of the system was small compared with the height of the flask. The flask top surface was therefore significantly out of focus. Furthermore, the field of view in the plane of the top of the flask was only 24 × 16 mm, so the edges of the top of the flask did not appear in the image. This arrangement significantly reduced image clutter and allowed a good view into the corners of the flask. As can be seen in figure 1, the bottom edge of the flask was visible around the outside of the image and colonies could be identified both inside and outside this border.

Standard culture flasks of type T25 with a flat bottom surface measuring 68 × 40 mm were used in all experiments. These were located under the camera with a simple jig consisting of three locating screws and a spring. The jig ensured that the culture flask was always in a reproducible position below the camera. Prior knowledge about the approximate position of the flask was used to aid the removal of flask structure in later image processing.

The flask was illuminated from below by an electroluminescent film (Pacel 'blue-green' type) which provided extremely uniform illumination at a wavelength of around 520 nm, with bandwidth of approximately 80 nm. A white Perspex diffuser was used above the film to remove
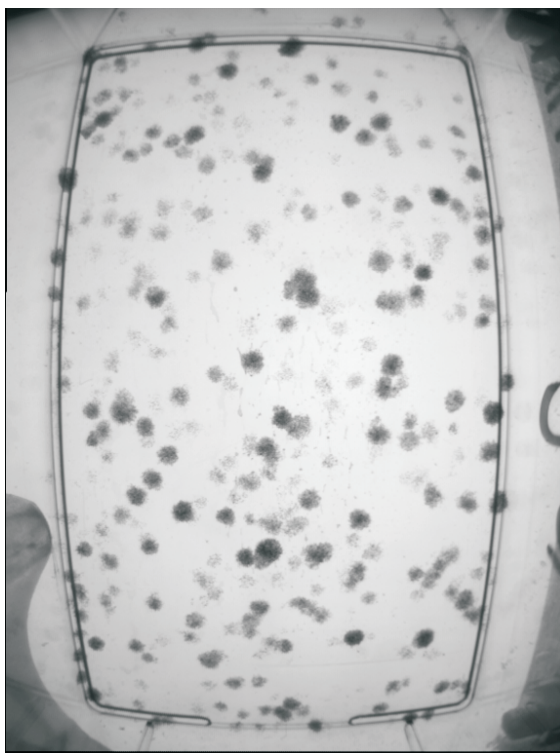
Figure 1. A typical image captured by the automatic colony counter showing colonies of cell type A172, many of which extend up the sides of the flask beyond the visible flask edge.

any slight imperfections in emission. This was protected by a 1 mm thick scratch-resistant, transparent plastic sheet (Edmunds type H43929). Illumination of this type gave optimal contrast for imaging cells stained with crystal violet, matching its absorption spectrum. The film was typically excited with a 150 V rms sine wave at 800 Hz, with the amplitude set to just produce 'peak white' in the camera. This drive waveform was derived from the camera frame rate (25 Hz) and phase-locked to it to ensure short- and long-term illumination stability.

Although the illumination was extremely uniform, the use of a wide-angle lens resulted in an apparent fall-off of illumination near the image edges, and gave rise to an effect similar to vignetting. This, however, could be easily removed with software where necessary. A typical image captured by the CCD camera is shown in figure 1. The imaging arrangement is shown in figure 2, where the close proximity of the illumination, flask and lens can be seen. External sources of light were excluded with a simple curtain shield.

The images were captured into the memory of a 450 MHz personal computer (PC) with a National Instruments (NI) IMAQ PCI-1408 image-capture board. The image was captured at a spatial resolution of 768 by 576 pixels and at an intensity resolution of 8 bits (256 levels), processed as a rectangular grid of square pixels.

2.3. Software

The software for the user interface and image processing was written in the C programming language. In all cases of image capture, 10 images were stored and averaged to reduce camera

Figure 2. The imaging arrangement showing the camera lens, a flask in the jig and the illuminating film below.

random noise effects. Before the images were processed to identify the colonies, the barrel distortion introduced by the wide-angle lens was removed using geometric distortion with bilinear interpolation (Gonzalez and Woods 1993). A quadratic distortion was assumed, centred on the image centre, and a magnification factor was also applied so that the images remain 768 by 576 pixels.

Two image-processing algorithms have been developed to detect and count cell colonies. Method 1 was developed first and is targeted at cell types that show good contrast with respect to the background but which may produce small colonies containing 10 to 20 pixels as well as large colonies with 1000 pixels or more. Colonies of these cell types, such as HT29, have little internal structure. The second image-processing method is aimed at very ill-defined or fuzzy colonies. These usually have very little contrast with respect to the background and may be large with significant internal structure. Example of such cell types include A172, U118 and IN1265. The choice of processing method for each cell type was made by eye. For the cell types tested it was obvious which method was most appropriate after applying both algorithms to two or three flasks of each type.
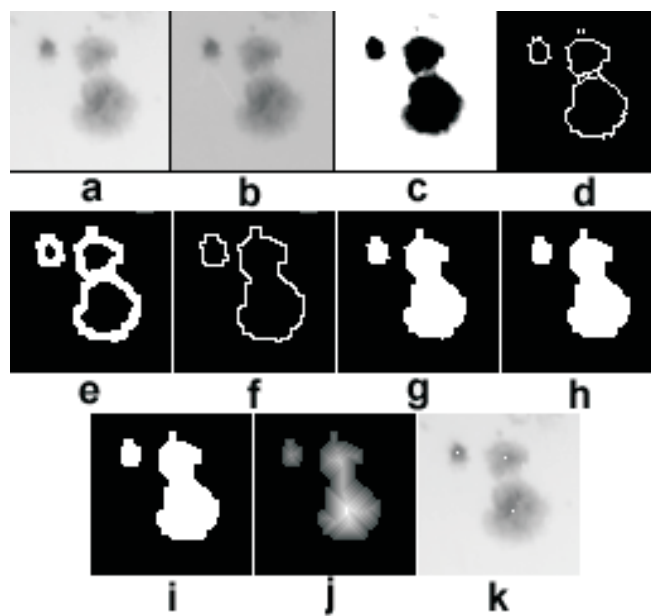
2.3.1. Image processing method 1. The first image-processing algorithm for colony counting works in a number of stages. A detailed description of each stage of the processing is given in this section.

The results of the processing at the 11 stages, a to k, of the algorithm are shown in figures 3 and 4 for cell lines HT29 and T98G. The cell line T98G is used as an example to show the performance of method 1 on less discrete colonies although the full results for this cell type are not presented. These figures show small portions (64×64 pixels) of the full processed image in order to reveal the detail of the processing. In both cases image portion a is the undistorted input image and image portion k shows the final result with each counted colony marked with a white dot.

An image of the stained flask is captured and is divided by the background image of an empty flask to remove the intensity variations and largely eliminate the structure of the flask edges. The resulting normalized image is used in further processing and is shown in image b of figures 3 and 4. The registration between the empty 'background' flask and the stained flask is never perfect because of imperfection in positioning the flask in the jig. Thus some remnants
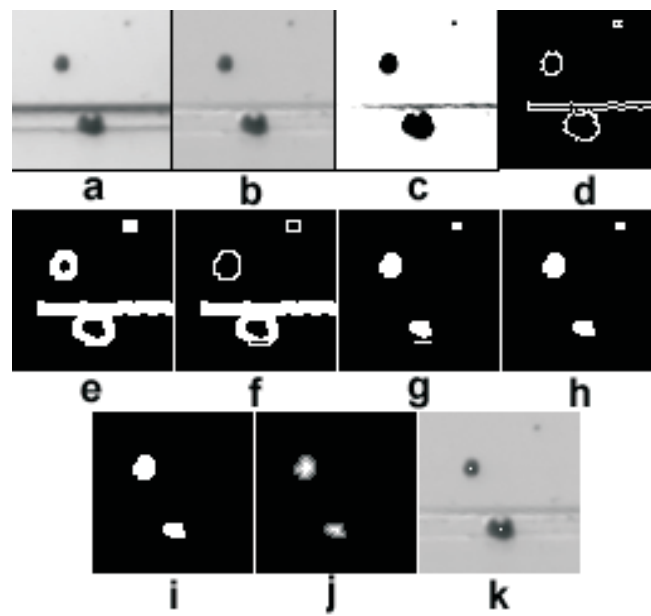
Figure 3. The result of applying image-processing method 1 on cell colonies of type HT29. The stages a to k are described in the text.

Figure 4. The result of applying image-processing method 1 on cell colonies of type T98G. The stages a to k are described in the text.

of the flask structure usually remain, but this is of greatly reduced contrast. The contrast of the image is increased just below the background level to enhance the borders of the colonies

(image c). The background grey-level value for the flask surrounding the colonies is estimated from the peak of the image histogram. Edge detection is performed to find all structure in the image (image d) and, in order to ensure these edges are four-connected, the image is dilated (image e). To avoid multiple detections due to the internal structure of some colonies, the external edges of all colonies known to be far from the flask edge are found by hole-filling and morphology (image f). Further hole-filling and image subtraction reveals the colonies as particles and this processing separates colonies from any structure due to the remaining flask edges (image g). Morphological filtering and discrimination on size and optical density ensure that only particles corresponding to colonies remain (images h and i). A distance function is calculated for each particle and the peaks in this function are found to separate overlapping particles (image j).

Further processing traces the flask edge to identify any small colonies so far missed because they are similar in size and density to the flask edge itself and thus are often hidden by it. Tracing the edge produces a one-dimensional signal along which high-pass filtering is performed to highlight additional colonies. The final result is shown in image portion k with colonies marked by white dots.

2.3.2. Image processing method 2.   An alternative algorithm has been aimed at fainter and ill-defined colonies, which have a tendency to overlap on the surface of the culture flask. The second method uses only the edge information of the image and a compact Hough transform approach to highlight the centres of circular objects. Our particular implementation of the compact Hough transform allows us to process images extremely quickly.

The first step is to find the edges using two perpendicular Sobel operators (Sobel 1990). A binary image of edge pixels (edgels) is produced by thresholding the edge magnitude. Each edgel is used to increment selected values in an accumulator space, as with any Hough transform, but it is the selection process that forms the key to this algorithm. It has already been shown (Mouroutis *et al* 1998) that circular shapes can be enhanced by incrementing the values in a half annulus around the position of the edgel in an approach similar to the generalized Hough transform (Ballard 1981). The disadvantage of this approach to our application is that straight lines are enhanced in addition to convex shapes, and incrementing in this way is also quite computationally intensive because of the need to calculate the annulus for every edgel. We would prefer circle-like objects to be enhanced and straight lines to be suppressed, and an algorithm that executes in seconds on current PC platforms. The algorithm described here is a novel implementation of the compact Hough transform that meets both the above requirements.

In our implementation, each edgel is associated with an incrementation of a line of values in accumulator space along a radius towards the dark side of the edge, as shown in figure 5. In the figure R_{min} and R_{max} specify the range of allowable colony radii in pixels which are determined by measuring the maximum and minimum colony size (selected by the user) encountered on a random sample of flasks. These parameters vary with the cell line used. The values on the dark side of the edge (the opposite to the edge direction) are incremented because we have prior knowledge that the colonies must appear dark on a bright background. Peaks in the resultant accumulator space correspond to the centres of circular objects since each edgel contributes to the accumulator value at the centre of its colony. The accumulator space is smoothed to remove small local maxima. The results of the processing steps described above are shown graphically in figure 6.

Any unwanted structure detected, for example at the rounded corners of the flasks, can be excluded by taking the transform of an image of an empty flask and subtracting it from the transformed image of the cell-containing flask. Since the image of an empty flask contains few
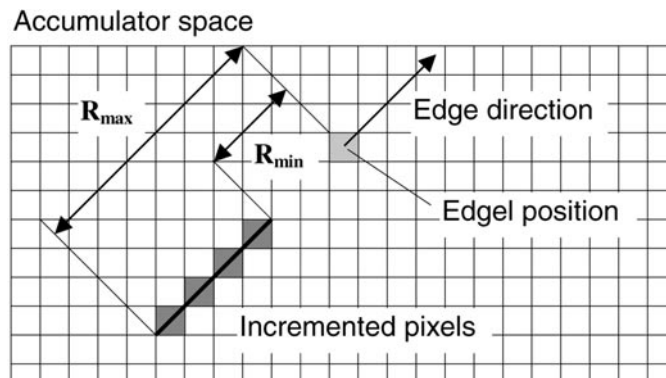
Figure 5. How the accumulator space is incremented by one edge pixel in this implementation of the compact Hough transform.
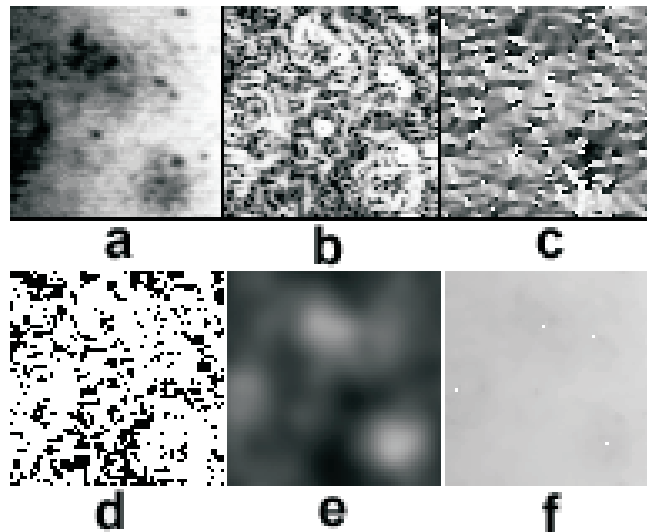

Figure 6. The result of applying image-processing method 2 on cell colonies of type IN1265. (*a*) A 64 × 64 pixel portion of the input image (histogram equalized). (*b*), (*c*) The edge magnitude (histogram equalized) and direction (encoded as a grey scale, 0–360° mapped onto 0–255). (*d*) Edgels thresholded from the edge magnitude (in white). (*e*) The result of the compact Hough transform using (*b*), (*c*) and (*d*). (*f*) Peaks in (*e*) represent colonies and are marked with white dots on the input image.

edges compared with the cell-containing flask, the added time taken for this step is reasonable for the benefit it gives.

The fast compact Hough transform runs in approximately 1 s on a 450 MHz PC, when processing 100 000 edgels, typically present in our colony images, from an image of 768 by 576 pixels. For comparison, the compact Hough transform using annuli requires over 200 s to run in the same conditions.

(a)

(b)

(c)

(d)
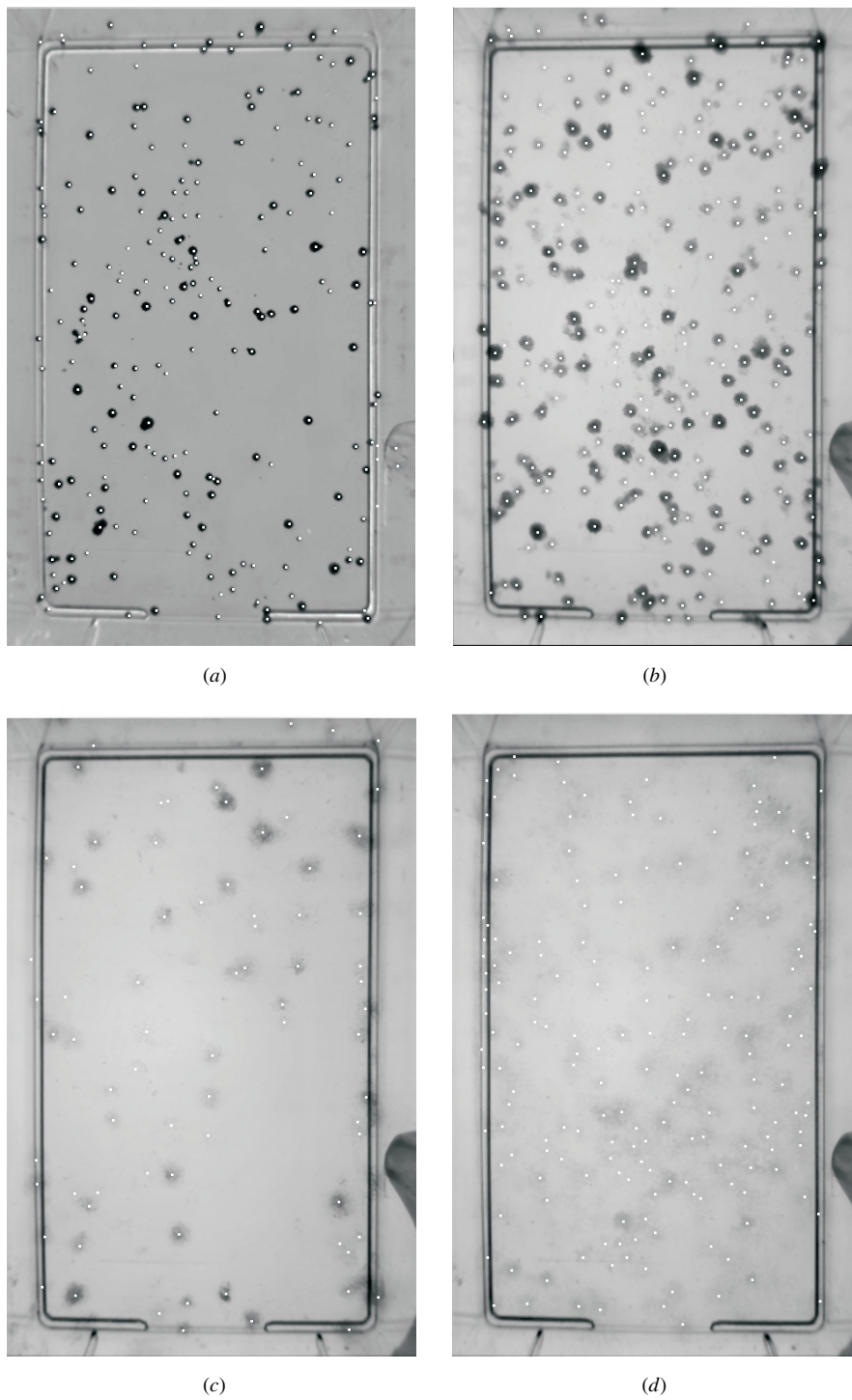
Figure 7. Example results of automated counting with processing method 1 on cell line HT29 superimposed on the original image with distortion and background removed (*a*), processing method 2 on cell lines A172 (*b*), U118 (*c*) and IN1265 (*d*) superimposed on the original image with distortion removed.
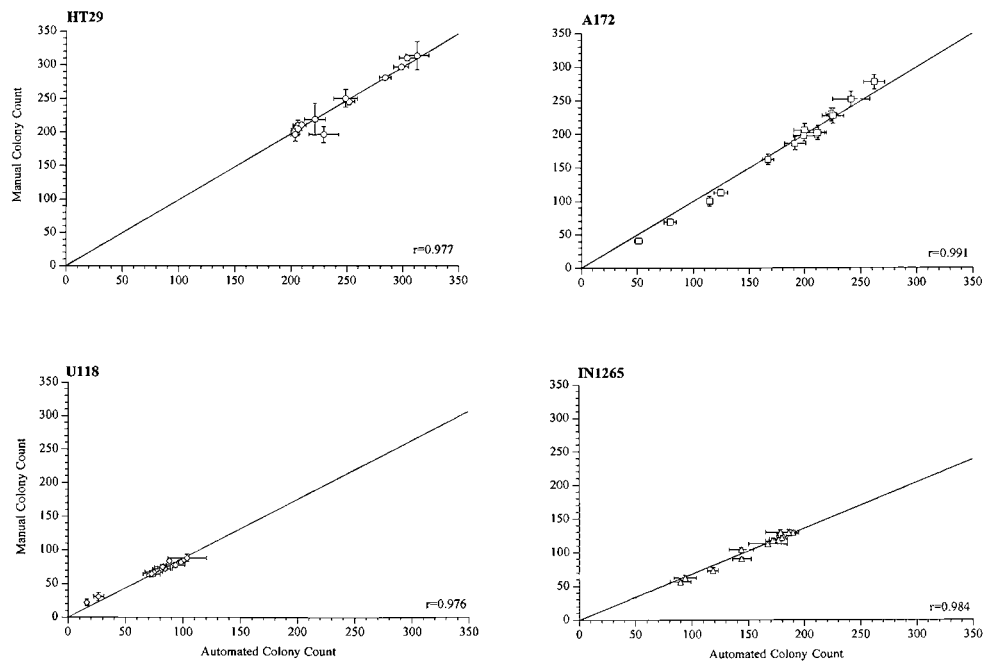
Figure 8. Correlation of the mean automated colony counts versus mean manual colony counts for HT29, A172, U118 and IN1265 cell lines. Each point represents the mean number of colonies counted ± the standard error of the mean for each dose. Regression lines through the origin are drawn and the correlation coefficients are shown in the bottom right-hand corner of each graph.
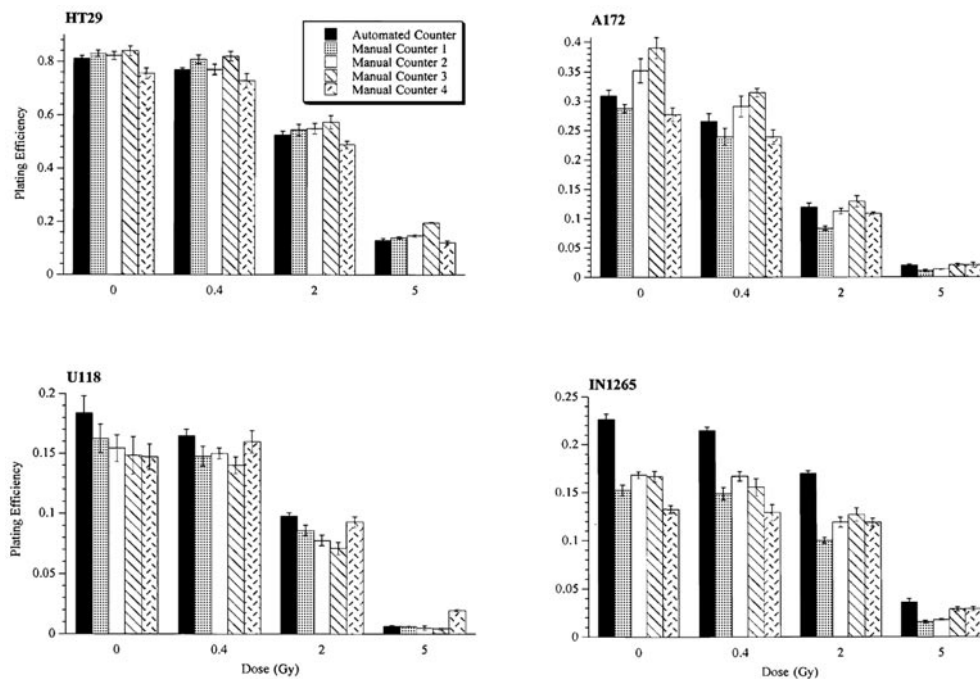
Figure 9. Plating efficiency (PE) for HT29, A172, U118 and IN1265 cell lines at four radiation doses (0, 0.4, 2 and 5 Gy). Each bar represents the mean PE ± standard error of the mean.

Table 1. P values following a t-test to compare manual plating efficiencies (PEs) in and surviving fractions (SFs) versus automated PEs and SFs at four doses for HT29, A172, U118 and IN1265 cell lines.

	Manual counter	Dose (Gy)							
		0		0.4		2		5	
		PE	SF	PE	SF	PE	SF	PE	SF
HT29	1	0.355	1	0.091	0.304	0.471	0.759	0.267	0.407
	2	0.585	1	0.956	0.677	0.366	0.512	0.090	0.118
	3	0.211	0.4305	0.038	0.079	0.167	0.226	0.001	0.001
	4	0.039	1	0.206	0.682	0.138	0.988	0.420	0.974
A172	1	0.121	0.635	0.247	0.690	0.008	0.017	0.010	0.015
	2	0.089	0.921	0.315	0.642	0.421	0.055	0.013	0.006
	3	0.003	0.707	0.033	0.308	0.452	0.154	0.915	0.118
	4	0.065	0.694	0.206	0.972	0.183	0.852	0.978	0.639
U118	1	0.210	0.275	0.170	0.170	0.089	0.089	0.676	0.676
	2	0.093	1	0.133	0.147	0.017	0.407	0.441	0.779
	3	0.091	0.767	0.054	0.828	0.010	0.116	0.101	0.320
	4	0.045	1	0.684	0.055	0.382	0.040	0.0002	<0.0001
IN1265	1	<0.0001	1	<0.0001	0.555	<0.0001	0.005	0.0004	0.010
	2	<0.0001	1	<0.0001	0.211	<0.0001	0.218	0.0007	0.011
	3	<0.0001	1	<0.0001	0.788	0.0002	0.790	0.1222	0.524
	4	<0.0001	1	<0.0001	0.715	<0.0001	0.002	0.1291	0.056

3. Results and discussion

Comparisons have been made between colony counts obtained from the automated colony counter and four manual observers for each experiment. Four experiments were performed using cell lines of different colony morphology. Each experiment involved either 45 (HT29, A172 and U118) or 84 (IN1265) flasks of stained colonies; this equates to three or six flasks at each of 13 doses plus six flasks at 0 Gy. Example results of automated colony counting are shown in figure 7 for the cell lines HT29, A172, U118 and IN1265 where each dot shows a colony counted overlaid onto the processed image. The results for cell line HT29 (figure 7(a)) have been overlaid onto the input image divided by the image of an empty flask as described in section 2.3.1. The values of R_{min} and R_{max} used with method 2 on cell lines A172, U118 and IN1265 were 3 and 8, 0 and 8 and 7 and 15 respectively. Figure 8 shows plots of mean automated counts at each dose versus person-averaged manual counts for each cell line. It can be seen that there was a strong positive correlation between the number of colonies counted automatically and manually for all four cell lines. The lines in the figure show a regression passing through the origin to demonstrate direct correlation. The true straight-line regression may reveal an offset in the automated count, which can be positive or negative, as well as a non-unity gradient. These may be due to the automated counter consistently over- or under-counting or due to the subjectivity of the human counters. Both effects are dependent on the colony morphology.

Figure 9 shows the mean PE at four doses for all four cell lines tested. In three of the four cell lines, most of the PEs obtained using the automated colony counter were not significantly different from those obtained by the four manual counters (table 1). This indicated that similar numbers of colonies were being recognized both manually and automatically. However, in the case of cell line IN1265, the automatic counts were higher than the manual counts and
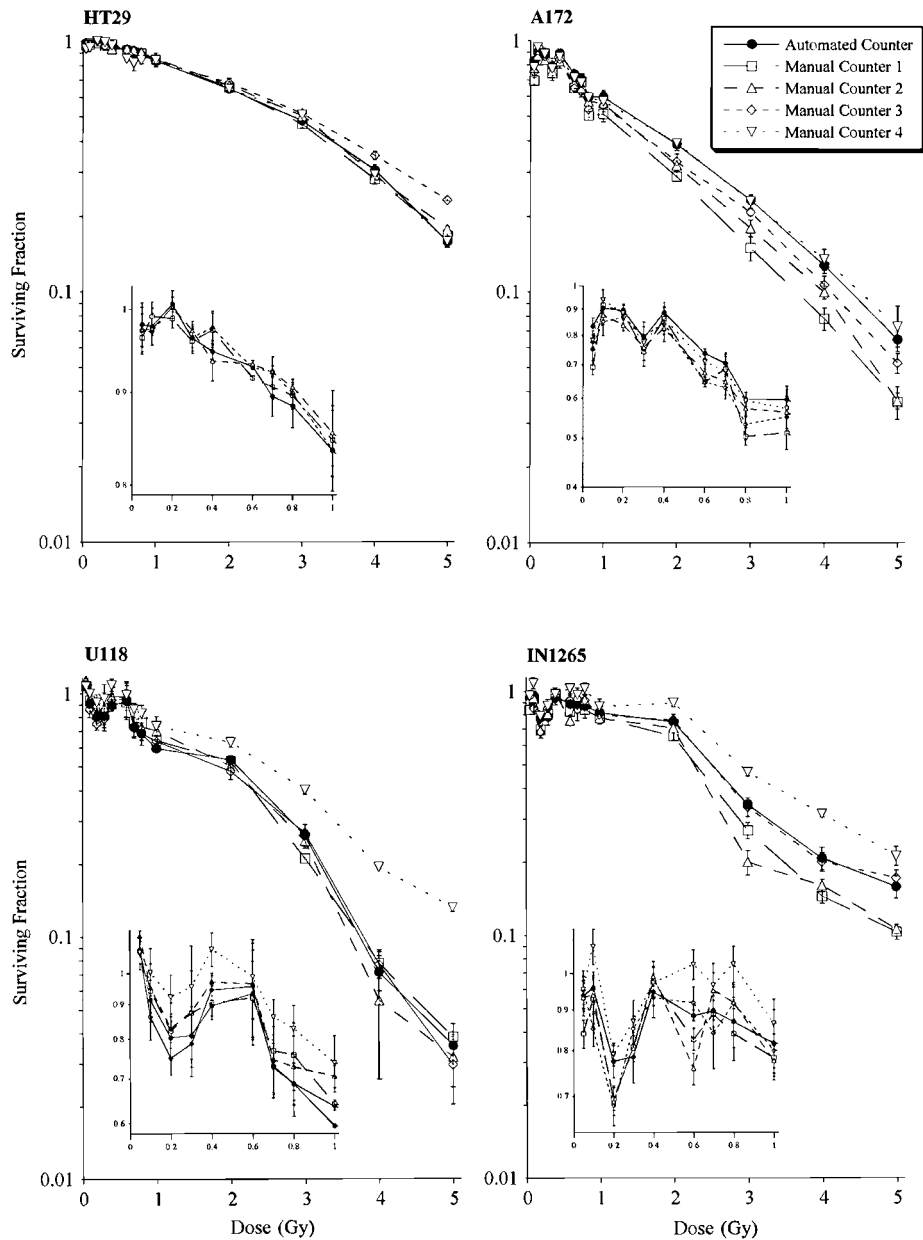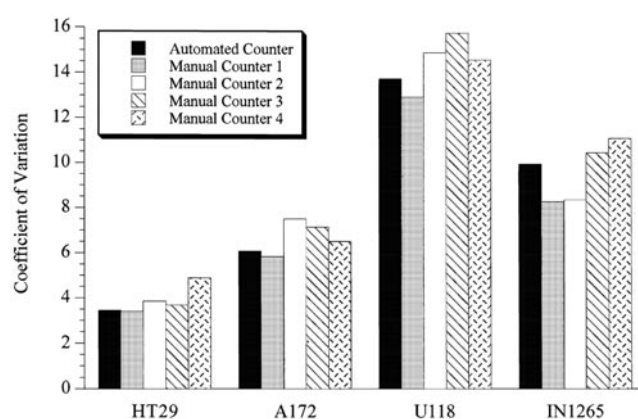
Figure 10. Survival curves of HT29, A172, U118 and IN1265 cell lines. Each graph shows five curves, one for each 'counter', with the results for the automated counter shown as full circles.

subsequent PE values significantly higher. This cell line has very ill-defined colonies and the automatic counter seemed to be multiply counting colonies which were counted as single by the manual counters; this in indicated by both figures 8 and 9.

Individual survival curves were then plotted for the five sets of counts obtained for each of the four cell lines in figure 10. This accounted for any differences between the absolute number of colonies counted by each operator corrected for the plating efficiency. Small variations in

Table 2. Comparison of the surviving fraction at 2 Gy (SF_2) and area under the curve (Dbar) values of HT29, A172, U118 and IN1265 cell lines obtained by automated and manual colony counting. Mean values and coefficient of variation (CV) are shown.

	Cell line							
	HT29		A172		U118		IN1265	
	SF_2	Dbar	SF_2	Dbar	SF_2	Dbar	SF_2	Dbar
Automated counter	0.660	3.07	0.361	1.95	0.498	2.01	0.669	2.76
Manual counter 1	0.663	3.07	0.260	1.45	0.386	1.82	0.571	2.40
Manual counter 2	0.680	3.17	0.273	1.52	0.452	2.07	0.605	2.38
Manual counter 3	0.720	3.42	0.265	1.48	0.416	1.95	0.656	2.76
Manual counter 4	0.642	3.13	0.315	1.70	0.612	2.74	0.807	3.35
Mean	0.673	3.17	0.295	1.62	0.473	2.12	0.662	2.73
CV	0.044	0.409	0.146	0.129	0.187	0.170	0.137	0.144

Figure 11. Coefficient of variation (CV) of the surviving fraction for HT29, A172, U118 and IN1265 cell lines. Each bar represents the CV of an individual counter's survival curve.

the survival curves of all four cell lines were observed and this appeared to be related to colony morphology. Thus the more discrete the colonies, the less interoperator variation was seen between survival curves, probably because counting this type of cell morphology is less subjective.

At higher radiation exposures (3–5 Gy), some cell lines exhibit significant changes in their colony morphology. This can cause variations in colony counting. As a result, significant differences in SF values were observed at 2 Gy and 5 Gy when p values were calculated between the automated and the four manual counts (table 1). However, the differences between individual counters, either automatic or manual, were small when the SF_2 (surviving fraction at 2 Gy) and Dbar (area under the curve) values were calculated (table 2).

Analysis of variance was used to determine an overall coefficient of variation (CV) of the SF values for the five counts made on all four cell lines (figure 11). The CV was based on the normalized intradose variability averaged over dose and gives an overall figure of merit for an experiment (smaller values indicating less error throughout the experiment). In three of the four cell lines, the CV of the automated results was ranked second best, and in the other cell line it was ranked third. This indicated that the automated counter appeared to be objective and consistent in colony counting ability.

The results show that the automated colony counter is able to produce SF measurements consistent with manual counters for cell lines with colonies as ill-defined as those for IN1265. The effect of a non-unity gradient in figure 8 is evident in when calculating PE (see figure 9) which is more noticable with the IN1265 cell line. However, its effect is removed when SF and Dbar values are calculated.

Any counting offset in figure 8 will cause errors in the automatically derived SF and Dbar values, but we see from the CV results of figure 11 that its effect is not significantly larger than similar errors between the manual counts. Further work should be aimed at counting accuracy in order to reduce such errors but the problem of identifying a 'gold standard' by which to judge performance will then become prevalent.

The average time to process flasks using the automated colony counter was approximately 30 s per flask, including the time taken to manually load and unload the flask from the unit.

Acknowledgments

References

Ballard D H 1981 Generalizing the Hough transform to detect arbitrary shapes *Pattern Recognition* **13** 111–22

Dobson K, Reading L and Scutt A 1999 A cost-effective method for the automatic quantitative analysis of fibroblastic colony-forming units *Calcified Tissue Int.* **65** 166–72

Gonzalez R C and Woods R E 1993 *Digital Image Processing* (Reading, MA: Addison-Wesley) ch 5

Hoekstra S J, Tarka D K, Kringle R O and Hincks J R 1998 Development of an automated bone marrow colony counting system *In Vitro Mol. Toxicol.* **11** 207–13

Lumley M A, Burgess R, Billingham L J, McDonald D F and Milligan D W 1997 Colony counting is a major source of variation in CFU-GM results between centres *Br. J. Haematol.* **97** 481–4

Marples B and Joiner M C 1993 Response of Chinese hamster V79 cells to low radiation doses: evidence of enhanced sensitivity of the whole cell population *Radiat. Res.* **133** 41–51

Mouroutis T, Roberts S J and Bharath A A 1998 Robust cell nuclei segmentation using statistical modelling *Bioimaging* **6** 79–91

Mukherjee D P, Pal A, Eswara S and Majumder D D 1995 Bacterial colony counting using distance transform *Int. J. Bio-Med. Comput.* **38** 131–40

Parry R L, Chin T W and Donahoe K 1991 Computer-aided cell colony counting *BioTechniques* **10** 772–4

Puck T T and Marcus P I 1956 Action of x-rays on mammalian cells *J. Exp. Med.* **103** 653–66

Short S C and Joiner M C 1998 Cellular response to low-dose irradiation *Clin. Oncol.* **10** 73–7

Short S C, Mayes C, Woodcock M, Johns H and Joiner M C 1999a Low dose hypersensitivity in the T98G human glioblastoma cell line *Int. J. Radiat. Biol.* **75** 847–55

Short S C, Mitchell S A, Boulton P, Woodcock M and Joiner M C 1999b The response of human glioma cell lines to low-dose radiation exposure *Int. J. Radiat. Biol.* **75** 1341–8

Sobel I 1990 An isotropic 3 × 3 image gradient operator *Machine Vision for Three-Dimensional Scenes* ed H Freeman (New York: Academic) pp 376–9

Spadinger I and Palcic B 1993 Cell survival measurements at low doses using an automated image cytometry device *Int. J. Radiat. Biol.* **63** 183–9

Thielmann H W and Hagedorn R 1985 Evaluation of colony-forming ability experiments using normal and DNA repair-deficient human fibroblast strains and an automatic colony counter *Cytometry* **6** 130–6

Wilson I G 1995 Use of the IUL Countermat automatic colony counter for spiral plated total viable counts *Appl. Environ. Microbiol.* **61** 3158–60

Wouters B G and Skarsgard L D 1994 The response of a human tumour cell line to low radiation doses: evidence of enhanced sensitivity *Radiat. Res.* **138** S76–S80